1 **Contributions of mechanical loading and hormonal changes to eccentric**

2 **hypertrophy during volume overload: a Bayesian analysis using logic-based**

3 **network models.**

4 Johane H. Bracamonte[1], Lionel Watkins[2], Pat Betty[3,4], Louis J. Dell'Italia[3,4], Jeffrey J.

5 Saucerman[2], Jeffrey W. Holmes[1,*]

6

7   (1) Department of Biomedical Engineering, University of Alabama at Birmingham,

8   Birmingham, Alabama, United States of America.

9   (2) Department of Biomedical Engineering, University of Virginia, Charlottesville,

10   Virginia, United States of America.

11   (3) Birmingham Veterans Affairs Health Care System, Birmingham, Alabama, United

12   States of America.

13   (4) Division of Cardiovascular Disease, Heersink School of Medicine, University of

14   Alabama at Birmingham, Birmingham, Alabama, United States of America.

15   (*) Corresponding author. Email: holmesjw@uab.edu

16

17

18 **Author Summary**

19 Mitral valve regurgitation is a common heart disease in which a malfunctioning valve

20 allows part of the blood pumped by the heart to flow in the wrong direction. This

21 condition overloads the heart by making it pump more blood volume than normal; the

22 heart temporarily adapts by growing in mass and volume, but if untreated the condition

23 can ultimately lead to heart failure and death. The most effective treatment is to

24 surgically repair the valve; however, in many patients heart function deteriorates even

25 after a successful surgery. Many researchers have studied this condition by

26 experimentally overloading the hearts of dogs and rats, producing large amounts of data

27 on the resulting geometric, mechanical, and biologic changes. Yet there is no clear

28 answer on how to prevent the progression of the disease. In this work we integrate

29 experimental data reported from 70 research articles on experimental volume overload

30 through a simple model of heart mechanics and a more complex model of the molecular

31 signaling pathways inside heart cells. We use a statistical approach to calibrate the

32 computational model, so that it can predict not only average responses but also the

33 degree of expected uncertainty for each prediction. We then use the model to explore

34 how the heart responds to potential treatments during overload.

35

Statements and Declarations

Competing interest:

The authors have no competing interests to declare that are relevant to the content of this article.

Availability of data and source codes:

Links to GitHub repositories containing all data and codes are provided within the text.

Authors contributions:

Conceptualization: Johane H. Bracamonte, Jeffrey W. Holmes

Data Curation: Johane H. Bracamonte, Betty Pat, Lou J. Dell'Italia

Formal Analysis: Johane H. Bracamonte, Lionel Watkins

Funding Acquisition: Johane H. Bracamonte, Jeffrey W. Holmes, Jeffrey J. Saucerman, Lou J. Dell'Italia

Investigation: Johane H. Bracamonte, Jeffrey W. Holmes, Betty Pat, Lou J. Dell'Italia

Methodology: Johane H. Bracamonte, Jeffrey W. Holmes, Jeffrey J. Saucerman

Project Administration: Jeffrey W. Holmes

Resources: Johane H. Bracamonte, Jeffrey W. Holmes, Jeffrey J. Saucerman, Betty Pat, Lou J. Dell'Italia

Software: Johane H. Bracamonte, Lionel Watkins, Jeffrey J. Saucerman

Supervision: Jeffrey W. Holmes

Validation: Johane H. Bracamonte, Jeffrey W. Holmes

Visualization: Johane H. Bracamonte, Lionel Watkins

Writing-original draft preparation: Johane H. Bracamonte

Writing-review and editing: Johane H. Bracamonte, Jeffrey W. Holmes, Jeffrey J. Saucerman, Lou J. Dell'Italia

70 **Abstract**

71 Primary mitral regurgitation (MR) is a pathology that alters mechanical loading on the

72 left ventricle and induces a distinctive ventricular remodeling response known as

73 eccentric hypertrophy. Drug therapies may alleviate symptoms, but only mitral valve

74 repair can provide significant recovery of cardiac function and dimensions. However,

75 20% of patients still develop systolic dysfunction post-operatively despite being treated

76 according to the current guidelines. Thus, better understanding of the hypertrophic

77 process in the setting of ventricular volume overload (VO) is needed to improve and

78 better personalize the management of MR. To address this knowledge gap, we employ

79 a Bayesian approach to combine data from 70 studies on experimental volume overload

80 in dogs and rats and use it to calibrate a logic-based network model of hypertrophic

81 signaling in myocytes. The calibrated model suggests that growth in experimental VO is

82 mostly driven by the neurohormonal response, with an initial increase in myocardial

83 tissue stretch being compensated by subsequent remodeling fairly early in the time

84 course of VO. This observation contrasts with a common perception that volume-

85 overload hypertrophy is driven primarily by increased myocyte strain. The model

86 suggests that Endothelin1 receptor activity plays a central role in driving hypertrophic

87 responses and the activation of the fetal gene program. The model reproduces a

88 number of responses to drug therapy not used in its calibration, and predicts that a

89 combination of endothelin receptor antagonist and angiotensin receptor blockers would

90 have the greatest potential to dampen cardiomyocyte hypertrophy and dysfunction in

91 VO.

92 **Author Summary**

93 Mitral valve regurgitation is a common heart disease in which a malfunctioning valve

94 allows part of the blood pumped by the heart to flow in the wrong direction. This

95 condition overloads the heart by making it pump more blood volume than normal; the

96 heart temporarily adapts by growing in mass and volume, but if untreated the condition

97 can ultimately lead to heart failure and death. The most effective treatment is to

98 surgically repair the valve; however, in many patients heart function deteriorates even

99 after a successful surgery. Many researchers have studied this condition by

100 experimentally overloading the hearts of dogs and rats, producing large amounts of data

101 on the resulting geometric, mechanical, and biologic changes. Yet there is no clear

102 answer on how to prevent the progression of the disease. In this work we integrate

103 experimental data reported from 70 research articles on experimental volume overload

104 through a simple model of heart mechanics and a more complex model of the molecular

105 signaling pathways inside heart cells. We use a statistical approach to calibrate the

106 computational model, so that it can predict not only average responses but also the

107 degree of expected uncertainty for each prediction. We then use the model to explore

108 how the heart responds to potential treatments during overload.

109

1. Introduction

Mitral valve regurgitation affects around 5 million people in America, and about 2% of the general population, with prevalence steeply increasing in individuals over 50 years of age [1]. In primary mitral regurgitation (MR) the dysfunction of one or more components of the valvular apparatus allows part of the blood volume pumped by the left ventricle to flow back to the low-pressure atrial compartment, making the heart pump a larger than usual volume of blood against a lower-than-normal resistance. The unique loading conditions imposed by MR induce a distinctive ventricular remodeling response known as eccentric hypertrophy, consisting of the lengthening of individual cardiomyocytes by addition of sarcomeres in series, leading to an organ-scale dilation of the left ventricle volume with little change in its wall thickness [2,3]. The neurohormonal response to volume overload is characterized by the activation of the sympathetic and renin-angiotensin systems, similar to other forms of cardiac overloading [4–6]. If MR is severe enough or if it remains untreated for long enough, the condition can transition from a compensated asymptomatic stage into irreversible heart failure with systolic dysfunction, a condition where the heart is unable to supply sufficient cardiac output to the body [7,8].

Drug therapies for heart failure due to primary MR alleviate symptoms and slow its progression, but only mitral valve repair can provide significant recovery of cardiac function and dimensions [2,9]. This fact has led clinicians to operate earlier in the national course of primary MR; yet 20% of patients still develop systolic dysfunction post-operatively despite being treated according to the current guidelines [10,11]. This fact highlights our incomplete understanding of eccentric hypertrophy due to primary

133 MR and its transition into systolic dysfunction and heart failure. A better understanding

134 of this process is needed to improve and better personalize the management of MR.

135 Most computational models of growth and remodeling during volume overload have

136 focused on the role of myocyte overstretch in driving eccentric hypertrophy [12,13]. By

137 contrast, molecular studies have shown reduced activity in stretch-sensitive myocyte

138 signaling pathways during experimental volume overload, the opposite of what would be

139 expected if remodeling is driven by stretch [14–18]. We hypothesized that this apparent

140 paradox might stem from complex interactions between hypertrophic signaling

141 pathways triggered by stretching and those that respond to other hormones and growth

142 factors known to be upregulated during volume overload.

143 Here, we employ a Bayesian approach to combine the wealth of available data on

144 experimental volume overload in dogs and rats using a logic-based network model of

145 hypertrophic signaling in myocytes, with the goal of better understanding the relative

146 influence of multiple factors that influence eccentric hypertrophy. We employed data

147 from 70 studies of experimental volume overload to estimate the probability distribution

148 of input parameters for a network model of hypertrophic signaling in cardiomyocytes

149 during volume overload, accounting for evolving levels of mechanical strain and

150 circulating hormones such as norepinephrine (NE), angiotensin II (AngII), and atrial

151 ANP and brain (BNP) natriuretic peptides. We then validated the ability of the calibrated

152 model to reproduce features of volume overload not included in the calibration, as well

153 as experimental responses to relevant independent experiments such as infusion of

154 hormones that induce myocyte hypertrophy.

155   The calibrated and validated model developed here represents a probabilistic, model-

156   driven meta-analysis of a large body of data on volume-overload hypertrophy, and as

157   such may be useful for screening future pharmacologic interventions [19]. We briefly

158   explored this potential by simulating several combinations of receptor blockades and

159   protein knockdowns to assess their effect on cardiomyocyte size in the setting of

160   volume overload. Our analysis suggests that elevated levels of circulating hormones

161   drive much of the hypertrophic response during late stages of experimental volume

162   overload, and that hormone-driven growth can reduce myocyte strain levels below

163   baseline despite elevated left ventricular volumes. These results contrast with the

164   assumption of most computational models that elevated myocyte stretch drives

165   eccentric hypertrophy but agree with much of the available molecular and signaling

166   data. A screen of potential pharmacological interventions suggests that a combination of

167   endothelin receptor antagonists and angiotensin receptor should have the potential to

168   reduce VO-induced hypertrophy. However, these simulations also identify situations

169   such as β adrenergic blockade where accurate predictions will require a multiscale

170   approach that considers both direct effects on hypertrophic signaling as well as indirect

171   effects through changes in mechanics and hemodynamics.

172   **2. Methods**

173   2.1.   Data collection

174   We reviewed and collected data from 37 research articles on experimental mitral

175   regurgitation in dogs and 33 articles on experimental volume overload in rats by aorto-

176   caval shunt. All data employed for our quantitative analysis were reported as a mean

177   value and standard deviation, so we assumed a normal probability distribution function

178   (PDF) for all measurement-derived variables. For the estimation of myocardial stretch at

179   tissue scale, we focused on canine experiments to avoid confounding effects of growth

180   in body size and weight common during experimental volume overload in rodents. We

181   collected data on changes in left ventricular (LV) mass, end-diastolic volume (V_{ED}), and

182   free wall thickness (h_{ED}), as well as previously reported estimates of end-diastolic

183   myofiber stretch in healthy dogs (λ_{ED}^0).

184   Both experimental VO and naturally occurring MR in dogs trigger elevated circulating

185   levels of multiple hormones relevant to hypertrophic signaling, including AngII, NE, ET-

186   1, NE, ANP and BNP. We collected all data on plasma or serum concentrations of these

187   hormones reported in the reviewed articles. All these species correspond to input nodes

188   in the cardiomyocyte network model. We also collected data reported in the studies we

189   reviewed on activity and phosphorylation levels of intracellular signaling proteins from

190   Western blotting on myocardial tissue extractions at several stages of VO. Specifically,

191   we collected data on focal adhesion kinase (FAK), Akt, ERK5, ERK12, ELK1, cGMP,

192   p38, and JNK, corresponding to intermediate nodes in the cardiomyocyte signaling

193   model. Additionally, we collected data on the abundance of proteins that are

194   synthesized by myocytes in tissue samples extracted following chronic VO and

195   correspond to output nodes in the model, including SERCA, Myosin heavy chain

196   isoforms αMHC and βMHC, ANP and BNP [20].

197   A detailed list of sources for all the collected quantitative data is summarized in the

198   supplementary material S1.1.

199   2.2.   <u>Integration of canine and rat experimental data</u>

200 Plots of the experimental fold change of normalized LV mass to body mass (LVM/BM)

201 during volume overload showed very similar shapes for dogs and rats, but hypertrophy

202 occurred much faster in rats [8]. When we fitted data from each species with an

203 exponential function and normalized the time axis by the time constant of that fit, we

204 found that data from both species aligned (Fig 1a, the full list of data sources is shown

205 in supplementary material S1.1). We therefore normalized all time course data in this

206 study by the time constant for each species. This allowed the use of combined data

207 from both animal models in our quantitative analysis.
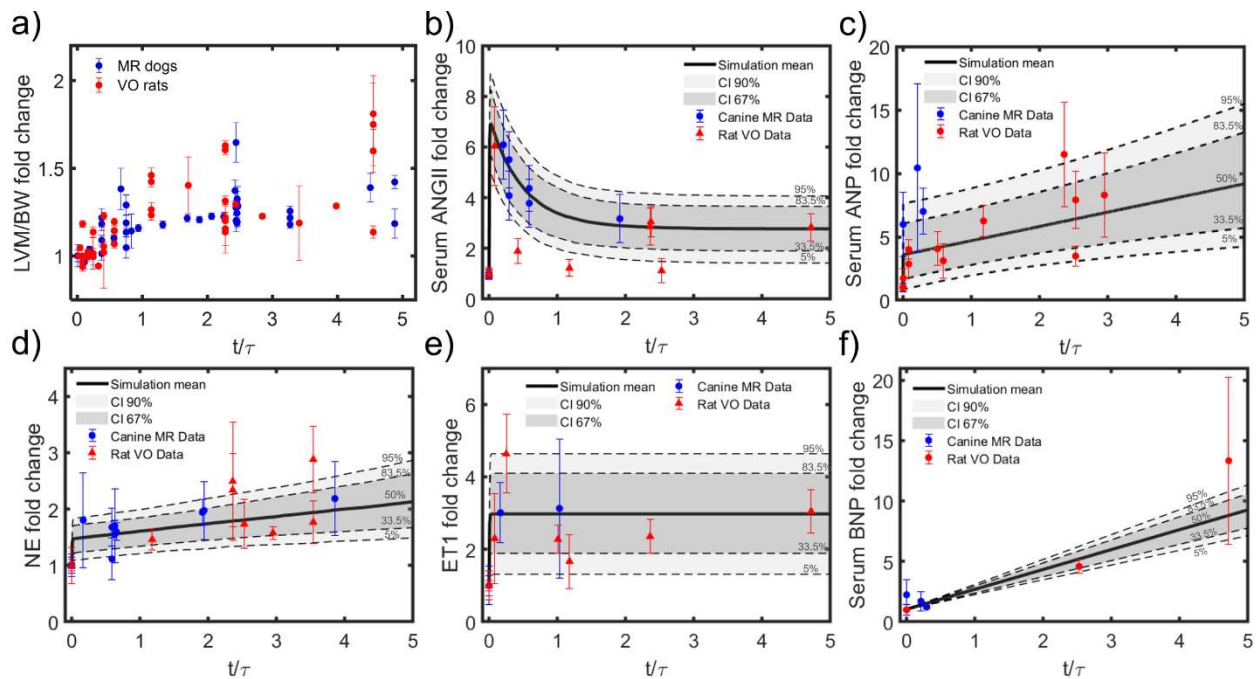
208

209 **Fig 1.** Integration of experimental data of MR in dogs and VO in rats. a) Fold changes in
210 LVM/BW over time normalized to each species characteristic growth-time constant. Data-
211 informed time-varying probability distributions of fold changes in circulating concentration of b)
212 angiotensin II (ANGII), c) atrial natriuretic peptide (ANP), d) norepinephrine (NE), e) endothelin
213 1 (ET1), and f) brain natriuretic peptide (BNP). References for all experimental datapoints
214 summarized in supplementary table S1.1 and fitted equations in table S1.3.

215

216

217

218   ## 2.3.   Time-varying hormonal input curves

219   We found baselines or control values of relevant hormone concentrations in blood were

220   consistent across animal sizes and species, suggesting a common homeostatic range

221   of circulating concentrations for each hormone. In this work, we assume that fold-

222   changes in concentration levels of those circulating hormones represented the intensity

223   of the neurohormonal response and would trigger proportional changes in the hormone-

224   receptor reaction input in the cardiomyocyte signaling model. The time resolved data of

225   serum concentrations were normalized to their corresponding baseline or control

226   concentration and plotted as a function of characteristic growth time (t/τ). We confirmed

227   that data from both species followed similar trends and fitted the integrated

228   experimental data with the simplest function that captured the temporal trends (Fig 1).

229   Details of the fitting process and the specific function fitted input dataset curved are

230   provided in the supplementary material section S1.2. and table S1.3 respectively.

231   ## 2.4.   Time-varying strain input curves

232   We assumed that changes in tissue-scale mechanical strain are proportionally

233   transduced to changes in the stretch input of the cardiomyocyte signaling model. Unlike

234   hormone concentrations, myocardial strain is a relative measure whose evolution over

235   time cannot be directly calculated from most published studies, so we must rely on a

236   mechanical model of the ventricular chambers to estimate strain from published

237   measurements. For the estimation of myofiber stretch, we assume the left ventricle to

238   be a thin-walled sphere. This oversimplification is not appropriate for some purposes

239   such as computing wall stress, but spherical models do capture the relation between

240   end diastolic volume and sarcomere length (Fig 2) [21], as well as the most salient

241   features of left ventricle pressure-volume behavior [22], and form the core of successful

242   published phenomenological models of ventricular hypertrophy [23]. Consistent with

243   most studies of low-pressure VO, we also assume pure eccentric hypertrophy, that is,

244   all mass increments are deposited in the fiber direction while neglecting the thinning of

245   the LV walls reported in some studies [24–26].

246
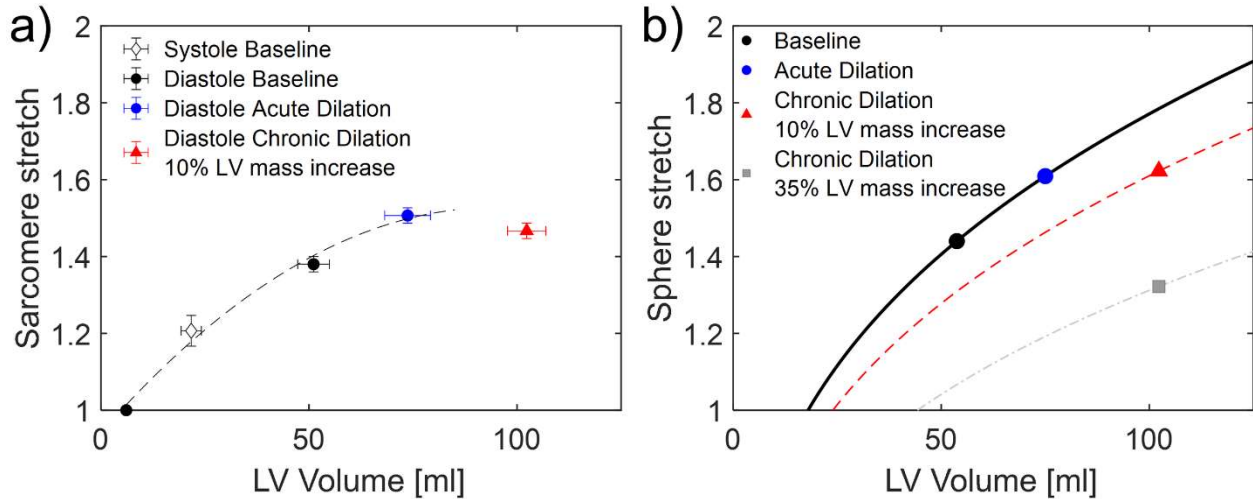
Fig 2. Spherical ventricular model correspondence to cardiomyocyte mechanics. a)
Experimental measurements of sarcomere stretch in dog hearts under physiological loading
conditions, in acute volume overload (Acute dilation) and long-term volume overload after 10%
LV mass growth. Figure adapted from Ross et al. (1971) [21]. b) Replication of baseline, acute
VO, and long-term VO conditions at diastole with a spherical ventricle model. The spherical
model displays reasonable correspondence to experimental measurements at cellular scale.
Notably, for a given amount of ventricle volumetric dilation an exacerbated increase in
ventricular mass may bring sphere stretch below the baseline.

256   With these assumptions, the myofiber strain can be estimated at any time (t^i) as:

$$\varepsilon_{ED}^i = \frac{1}{2}\left[\left(\frac{V_{ED}^i}{V_0^i}\right)^{2/3} - 1\right], \qquad (1)$$

257   where V_{ED}^i is the end-diastolic volume at a given time, and V_0^i is the hypothetical

258   unloaded (zero-pressure) volume. While the end-diastolic volumes V_{ED}^i are reported in

259   the studies reviewed here or can be calculated from reported dimensions, changes in V_0^i

260   must be estimated from reported changes in LV mass (Supplementary material S1.3).

261   The unloaded volume prior to the onset of overload (V_0^0) was estimated based on

262   previous calculations of in vivo end diastolic stretch (λ_{ED}^0) [27], as well as zero-pressure

263   ventricular volumes reported from experiments on healthy dogs [28]. A detailed

264   derivation of strain probability distribution functions from experimental data is provided

265   in Supplementary material S1.3.

266   Once calculated, strain was mapped to the network input myoStrain with an exponential

267   function:

$$w_{myoStrain} = C_{myoStrain}(e^{D_{myoStrain}\,\varepsilon_{ED}} - 1) \quad (2)$$

268   ### 2.5.   Model of cardiomyocyte hypertrophic signaling pathways

269   We employed a published computational model of the hypertrophy signaling network

270   that integrates many established pathways implicated in cardiac myocyte growth. The

271   model consists of a logic-based network where the activity of each node follows a

272   normalized Hill equation with possible activity values ranging from 0 and 1 [20,29]. The

273   network consists of 106 nodes representing hormones and intracellular molecules and

274   192 reactions. The model has been used previously in the study of ventricular

275   hypertrophy and was recently optimized in the context of β adrenergic stimulation [30].

276   The set of network parameters is summarized in supplementary table S2. In

277   supplementary figure S1.1 we show a representation of the network model highlighting

278   the nodes with available experimental data.

279   The influence of a reaction on the downstream nodes is modulated by the weight

280   parameter w, which was left at the default value for all nodes except the inputs for

281   AngII, ANP/BNP, ET1, NE, and stretch. The characteristic time constant governing the

282   speed of changes in node activity was chosen as 0.005τ, for all intracellular reactions

283 and 0.02τ for output nodes reflecting protein synthesis, where τ is the fitted time

284 constant for the exponential rise in LV mass, as discussed above. The network model

285 was solved with Netflux (https://github.com/saucermanlab/Netflux). More detail about

286 the network model formulation and solution method can be found in [31].

287   2.6.   <u>Bayesian inference analysis of experimental data</u>

288 All parameter estimations required in our data processing pipeline were performed

289 within a Bayesian inference framework. The Bayesian inference tool utilized for this

290 study was a standard Markov Chain Monte Carlo (MCMC) algorithm with Metropolis-

291 Hasting selection criteria and Gibbs sampling to navigate the multiparametric space.

292 Briefly, the algorithm iteratively solves a numerical model while randomly varying its

293 input parameters over a predetermined probability distribution, known as the prior

294 probability distribution function (prior PDF) of the parameter space. On each iteration,

295 the likelihood of the model's outputs is evaluated against experimental data. If the

296 likelihood of the outputs with the current parameter set is larger than the likelihood of

297 the previous iteration, the parameter set is saved. If the outputs for the current

298 parameter set are less likely, the decision on whether to save the current parameter set

299 is made randomly. After sufficient iterations, the collection of saved parameter sets

300 converges to a new probability distribution of the parameter space, or posterior PDF,

301 which are associated with probability distributions for the model predictions [32,33].

302 In this study, each MCMC algorithm was applied in two stages, first assuming a uniform

303 probability distribution of the parameters within their physiologically plausible limits for

304 10,000 iterations. The resulting posterior PDF was then used as the prior PDF for a

305 second run of the MCMC algorithm for additional 20,000 iterations, with a check to

306 verify the convergence of the solutions every 5,000 iterations (Supplementary material

307 S1.4). The MCMC algorithm was programmed in MATLAB calling on Netflux. The

308 source code including the transcript of experimental data is available at

309 https://github.com/cardiacbiomechanicsgroup/MCMC_cardiomyocyte_VO_growth .

310 *2.6.1. Probability distribution of hypertrophy network input weights*

311 The normalized time-varying curves of hormone concentrations and mechanical strain

312 provide information on how these stimuli vary over time but does not resolve their

313 relative influence on cardiomyocyte function. One advance of the current work over

314 previous applications of this network model is that we allow the key hypertrophic stimuli

315 to have different weights. In the cardiomyocyte signaling network model, the weight of

316 the hormone-receptor reaction determines its relative influence on the network for a

317 given fold change in that hormonal input. The time-varying influence of a given input is

318 calculated as the product of its baseline weight $\left(w^0_{species}\right)$ and its normalized time-

319 varying fold-change curve (sections 2.3 and 2.4), where $w^0_{species}$ is unknown. We

320 employed an MCMC to estimate the PDF of the baseline weights of hormone-receptor

321 input reactions as follows. We first assumed a uniform prior PDF for the input weights of

322 ANGII $\left(w^0_{AngII}\right)$, NE $\left(w^0_{NE}\right)$, and ET1 $\left(w^0_{ET1}\right)$ reactions. Sampling was constrained within

323 the range for which the Cell Area output is sensitive to those inputs. Specifically,

$$0.01 < w^0_{ANGII} < 0.15$$

$$0.01 < w^0_{NE} < 0.24 \qquad (3)$$

$$0.01 < w^0_{ET1} < 0.17$$

324 For the rest of the hormone input reactions, we assign a single "background" reaction

325 weight, sampled within the $0.01 < w_{background} < 0.4$ range. A preliminary study revealed

326   that, within the range of interest, the input reaction weights of ANP and BNP to

327   Guanylate Cyclase A (GCA) receptors have only marginal effects on predicted changes

328   in Cell Area; we therefore prescribed ANP/BNP the same weight as the background

329   species. We assigned null weight to the synthetic drug phenylephrine and isoproterenol

330   (ISO) reactions except when simulating drug infusions. We fixed the weight of the

331   mechanical stimulus input $\left(w^0_{myoStrain}\right)$ at a single value for each MCMC run and

332   repeated the process for $w_{myoStrain}$ values of 0.02, 0.04 0.05 0.055, 0.06, 0.065, 0.07,

333   0.08, and 0.09. The MCMC also estimates the probability distribution for the tissue

334   strain-to-myoStrain mapping parameter $C_{myoStrain}$, while parameter $D_{myoStrain}$ is

335   calculated for each MCMC iterations with equation 2 and $w^0_{myoStrain}$ and ε^0_{ED}.

336   On each step of the MCMC, the algorithm randomly samples the w^0_{ANGII}, w^0_{NE}, w^0_{ET1},

337    $w_{background}$, $C_{myoStrain}$ parameter space and randomly selects time-varying curves for

338   each stimuli from their respective PDFs (Fig 1 and Fig 3c). The likelihood of the model

339   outputs was evaluated against the experimental data on FAK, Akt, ERK5, ERK12,

340   ELK1, cGMP, p38, and JNK activity and cardiomyocyte growth (CellArea) from dog and

341   rat experiments. We added a condition assigning larger likelihoods to parameter sets

342   that produce a baseline CellArea activity near 0.5, in the most responsive region of the

343   sigmoidal curve.

344   Long-term experiments agree that LV mass plateaus at a new level in chronic stages of

345   VO [34]. We therefore assumed that continued growth at late time points and negative

346   growth (reversal of hypertrophy) at any time point were very unlikely. After convergence

347   of the MCMC we filtered out these very unlikely solutions and recorded the posterior

348   PDFs of the activity of the network nodes of interest.
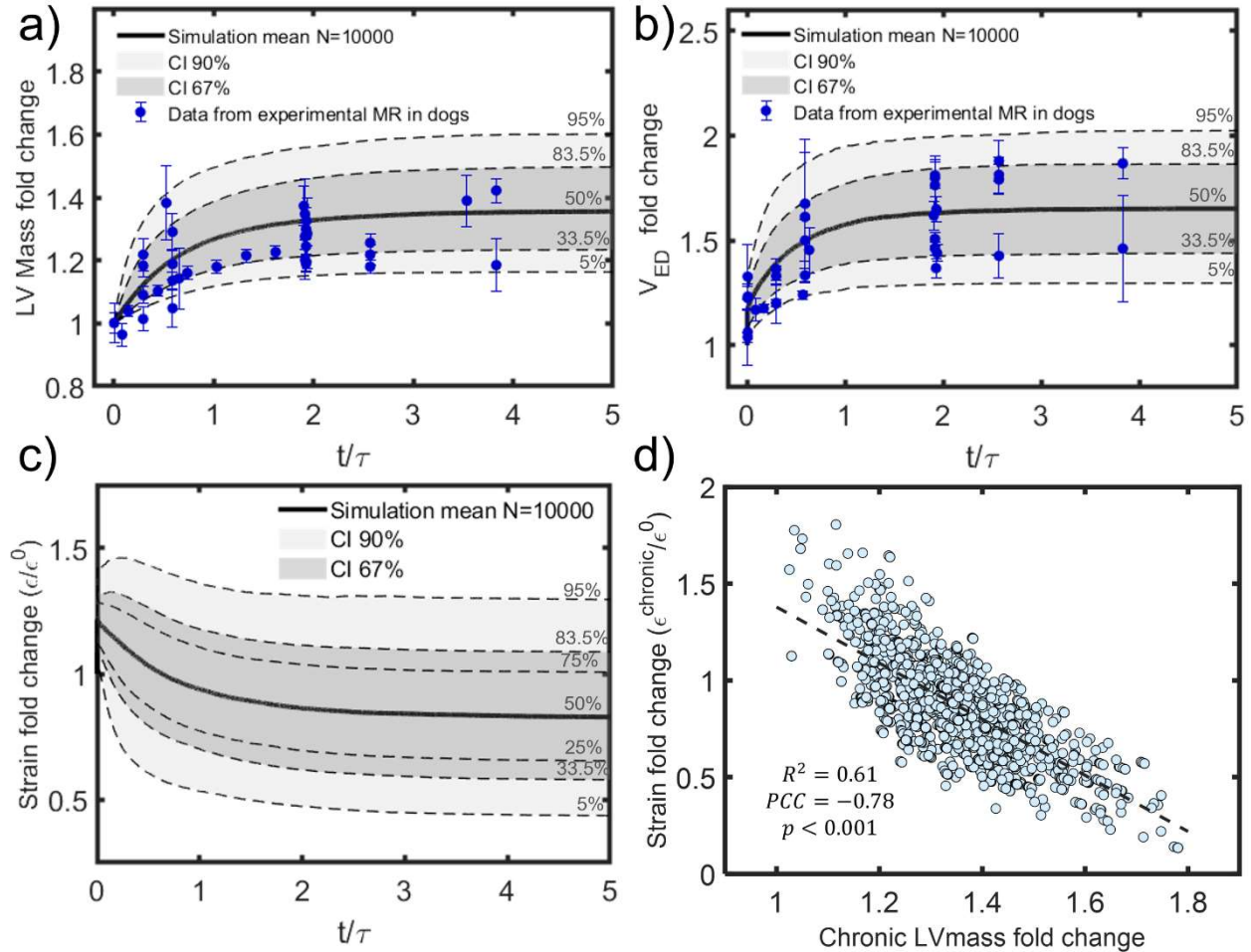
Fig 3. Results of the organ-scale data analysis. Time-varying probability distributions of a) LVM fold changes. b) End-diastolic volume (V_{ED}) fold changes, and c) Strain fold change. Influence of LVM and V_{ED} on the estimation of chronic fold changes in strain. LVM increment displays a strong inverse correlation with Strain changes. Sources for experimental measurements of LVM and V_{ED} are summarized in supplementary table S1.1.

2.7. Sensitivity analysis

We evaluated the sensitivity of network outputs (production of ANP, BNP, αMHC, βMHC, and SERCA) to the network inputs (weight of ANGII, NE, ET1, ANP and BNP to receptor reaction) by a standard correlation matrix based on statistical linear regression. The Pearson correlation coefficient (PCC) was calculated to quantify the parameter sensitivity. This method exploits the wealth of samples produced during the MCMC runs

362   to yield sensitivity estimates that are meaningful within the expected range of network

363   activity.

364   2.8.   <u>Validation of reaction weight posterior PDF</u>

365   Data corresponding to the network outputs ANP, BNP, $\alpha MHC, \beta MHC$, and SERCA were

366   not used in the estimation of parameter likelihoods during the MCMC runs. Thus, the

367   first round of validation consisted of comparing the estimated fold changes in activity

368   level of those output nodes to the corresponding fold changes in protein abundance

369   from experimental data.

370   We further validated the calibrated network model against data from independent

371   studies of *in vivo* drug stimulation of hypertrophy. For this, we performed *in silico*

372   replications of infusion experiments of ANGII in rats [35,36], NE in dogs [37–39], and

373   Isoproterenol (ISO) in mice [40] and compared the model-predicted changes in CellArea

374   to reported LV mass growth. We assumed that hormone infusion had no effects on

375   myoStrain.

376   The *in silico* replication consisted of increasing the input weight of the infused hormone

377   according to the circulating concentration fold-changes reported in experiments while

378   keeping the rest of the inputs at their baseline. Baseline values for the remaining inputs

379   were varied by sampling from their posterior PDFs over N=1000 iterations.

380   In the case of ISO infusion, a previous study by Estrada et al. determined that the

381   experimental dosages simulated here were sufficient to saturate the hypertrophic

382   response, so we imposed the maximum weight of 1 on the ISO node to simulate its

383   infusion.

384   2.9.   <u>Screening of pharmacological alternatives in the setting of VO</u>.

385   We explored pharmacological alternatives for the treatment of hypertrophy in mitral

386   regurgitation by using the calibrated and validated model to reproduce experimental VO

387   conditions while knocking down the activity of key network nodes. First, we explored

388   drug therapies conventionally used to treat heart failure: β-blockers, Angiotensin

389   Receptor Blockers (ARB), and endothelin receptor antagonists (ET1A), independently

390   and in paired combinations.

391   Next, we identified prospective non-conventional therapeutic targets by running a

392   knock-down sensitivity analysis. For this we set the network model to its mean activity

393   state for chronic VO, then ran iterative simulations in which we knocked down the

394   activity of individual network nodes one by one and recorded the effect on the CellArea

395   node. We calculated the knock-down sensitivity as $S_j = \left(\Delta y_{CellArea}/\Delta y_j \right)\left(y_j^0/y_{CellArea^0}\right)$,

396   where $\Delta y_{CellArea}$ and $y_{CellArea^0}$ are the change of activity and baseline activity of the

397   CellArea node respectively, and Δy_j and y_j^0 are the change in activity baseline activity of

398   the knocked-down species.

399   The effect of the drugs on VO-induced hypertrophy was assessed by running standard

400   Monte Carlo simulations (N=1000) with random samples over the PDF of baseline

401   reaction weights, and time-varying fold changes of hormone concentrations and strains

402   characteristic of VO, while assigning null activity to network nodes corresponding to the

403   drug action. Finally, we compared the predicted effect of conventional drugs on growth

404   to the reports by Sabri et al. and Pat et al. on β-blockers [15,16] Murray et al.

405   (2008,2009), Francis et al., and Lee et al. on ET1A [41–45] and Perry et al. and Zhang

406   et al. on ARB [26,46] (Supplementary table S1.2).

407   **3. Results**

408   3.1.   <u>Probability distributions of fiber strain.</u>

409   We produced a data-informed continuous probability distribution of end-diastolic strain

410   (ε_{ED}) relative to an unloaded state over the course of experimental VO. The PDF

411   display the expected trends over time, that is, an acute increase in strain owing to the

412   sudden increase of V_{ED}, followed by a gradual decrease driven by the compensatory

413   hypertrophic response (Fig 3). As V_{ED} and LVM curves reach a plateau in chronic VO

414   stages, ε_{ED} also stabilizes at a magnitude close to its baseline. Models in which

415   mechanical strain is the only promoter of cardiomyocyte growth only produce this stable

416   hypertrophied state if strain returns to its baseline level, or the homeostatic strain level

417   is allowed to adapt [13,47]. Interestingly, our data analysis suggests that in 75% of the

418   cases, strain falls below its original baseline level in chronic stages of experimental VO

419   (Fig 3c), with 50% of the cases passing below this threshold relatively early ($t/\tau \leq 1$

420   corresponding to the first 12 days in rats and 6 weeks in dogs). Myofiber strain showed

421   a strong inverse correlation to LVM fold change (PCC=-0.78), suggesting that myofiber

422   stretch falling below baseline is more likely to occur in cases with the greatest mass

423   increase (Fig 3d).

424   3.2.   <u>Cross-species data integration and probability distribution of hormonal stimuli.</u>

425   The best-fit characteristic time constant for mass growth is (τ_M) 1095 hours for dogs

426   and 283 hours for rats. The ratio of the species time constant is $\tau_{M_{dog}}/\tau_{M_{rat}} = 3.86$.

427   Interestingly, this ratio is close to the proportion between the heart rates (HR) of the

428   sampled populations, which is often used for allometric scaling [48]. With an average

429   HR of $363 \pm 14\ bpm$ for rats and $95 \pm 4\ bpm$ for dogs, the ratio is $HR_{rat}/HR_{dog} =$

430   3.82 ± 0.22.

3.3. Probability distribution of input stimuli reaction weights

In this section we present the results of the Bayesian analysis of the signaling network model and probabilistic fitting of its input parameters. Preliminary screenings of the parameter space revealed that the baseline weight of the myoStrain input $\left(w^0_{myoStrain}\right)$ greatly modulated the occurrence of experimentally unlikely solutions, such as growth reversal and runaway growth that never stabilized. We therefore ran a series of MCMCs with fixed $w^0_{myoStrain}$ while randomly sampling the rest of the input reaction weights as described in section 2.6.1. We found that constraining the baseline weight of the myoStrain input within the range $0.055 \leq w^0_{myoStrain} \leq 0.060$ minimized the number of unlikely solutions. For $w^0_{myoStrain} > 0.06$, the solutions tend to be dominated by the myoStrain input, resulting in a reversal of growth at later time points despite continuing simulated overload, while the solutions for $w^0_{myoStrain} < 0.05$ were dominated by adrenergic stimulation, increasing the chances of runaway growth (Supplemental material S1.5). The results presented here were therefore obtained with a fixed $w^0_{myoStrain} = 0.06$, which was associated with the highest mean likelihood among the myoStrain values we tested.

The posterior PDF of the remaining input reaction weights converged to:

$$w_{ANGII} = 0.010 \pm 0.002$$
$$w_{NE} = 0.033 \pm 0.014$$
$$w_{ET1} = 0.056 \pm 0.025 \tag{4}$$
$$w_{background} = 0.031 \pm 0.022$$

448   We calculated correlations among these inputs weights. The strongest correlation was

449   between w^0_{ET1} and $w^0_{background}$ with a Pearson PCC=-0.42, while all other PCC

450   magnitudes were below 0.3.

451   The network outputs were insensitive to the strain-to-myoStrain mapping parameters.

452   The PDF of the mapping parameter converged to $C_{myoStrain} = 5.86 \pm 1.38$.

453   3.4.   <u>Sensitivity analysis</u>

454   The sensitivity revealed that all network outputs were far more sensitive to ET-1 than to

455   any of the other network inputs examined in this study (Fig 4). This suggests that, in

456   chronic stages of VO, variation in ET-1 circulating concentrations within its probable

457   range has the largest influence on cardiomyocyte size and function of any individual

458   hormonal or mechanical growth factor. According to this analysis, higher levels of ET-1

459   in chronic stages of VO are associate with greater cardiomyocyte growth, greater

460   myocardial production of βMHC, ANP and BNP, and reduced myocyte synthesis of

461   SERCA and αMHC (Fig 4). This result is consistent with the knock-down sensitivity

462   analysis, where the elimination of ET-1 stimulation produced the largest change in

463   activity of multiple signaling nodes downstream of ET-1 including calcium, calmodulin

464   (CaM), CaM kinase, and mTor (Supplementary figures S1.10, S1.11). This result

465   implies that among the circulating hormones known to be altered during VO,

466   manipulating ET-1 levels, receptor-activity, or signaling should offer the greatest

467   potential to modulate hypertrophy and other myocardial responses to VO. This

468   hypothesis is explored further in Section 3.6 below.

469

470
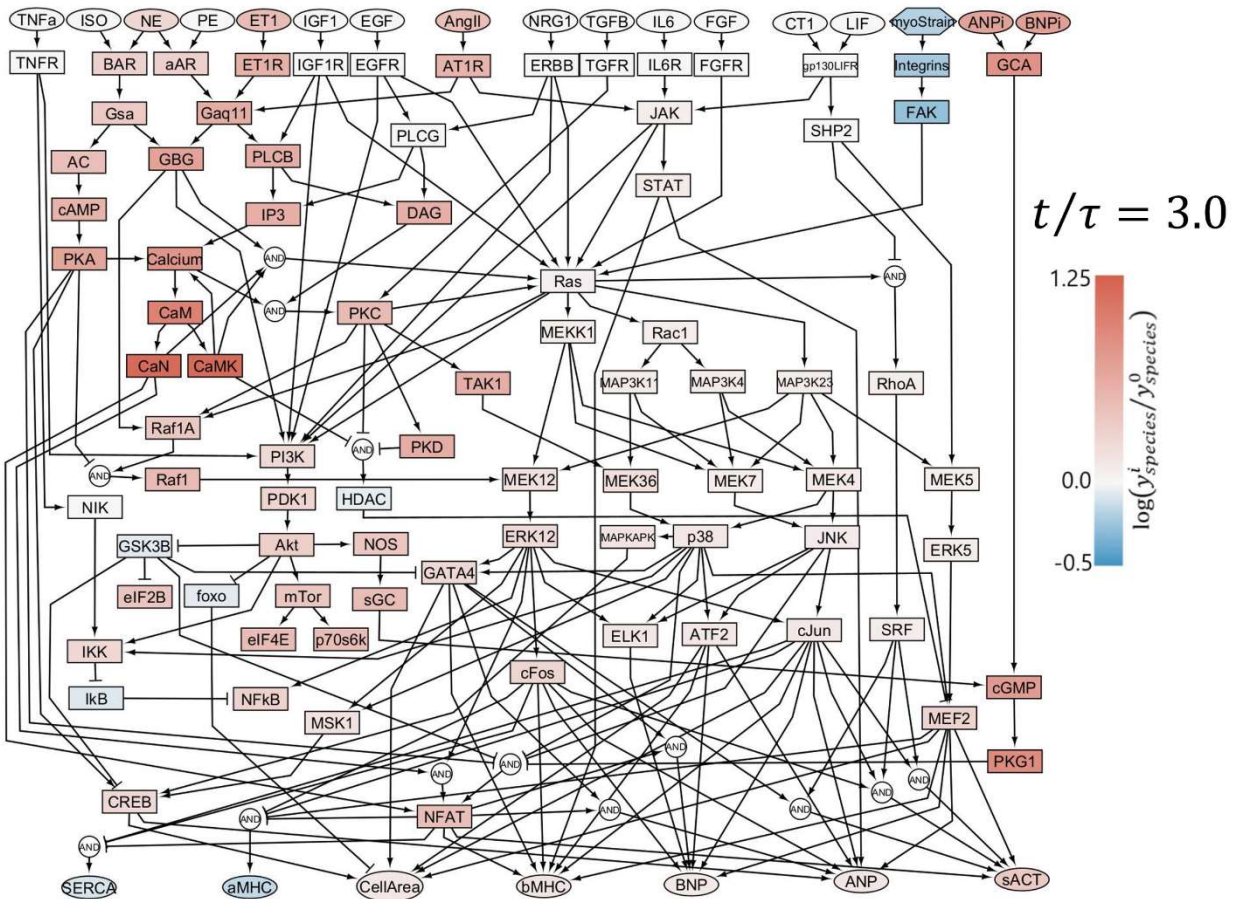
Fig 4. Sensitivity analysis of network outputs to inputs in chronic stages of chronic VO. Each marker represent the final state of a simulated VO experiment. A linear regression model (dashed line) is fit to each simulation-generated output-input pair. Pearson PCC is displayed on the upper left corner of each. The PCC represents the relative influence of inputs on each output, with ET1 displaying the largest influence on all outputs.

3.5. Validation

The calibrated model properly predicts the activation of the fetal gene program in the

context of experimental volume overload, including the downregulation of SERCA and

αMHC and upregulation of ANP, BNP, and βMHC (Fig 5).
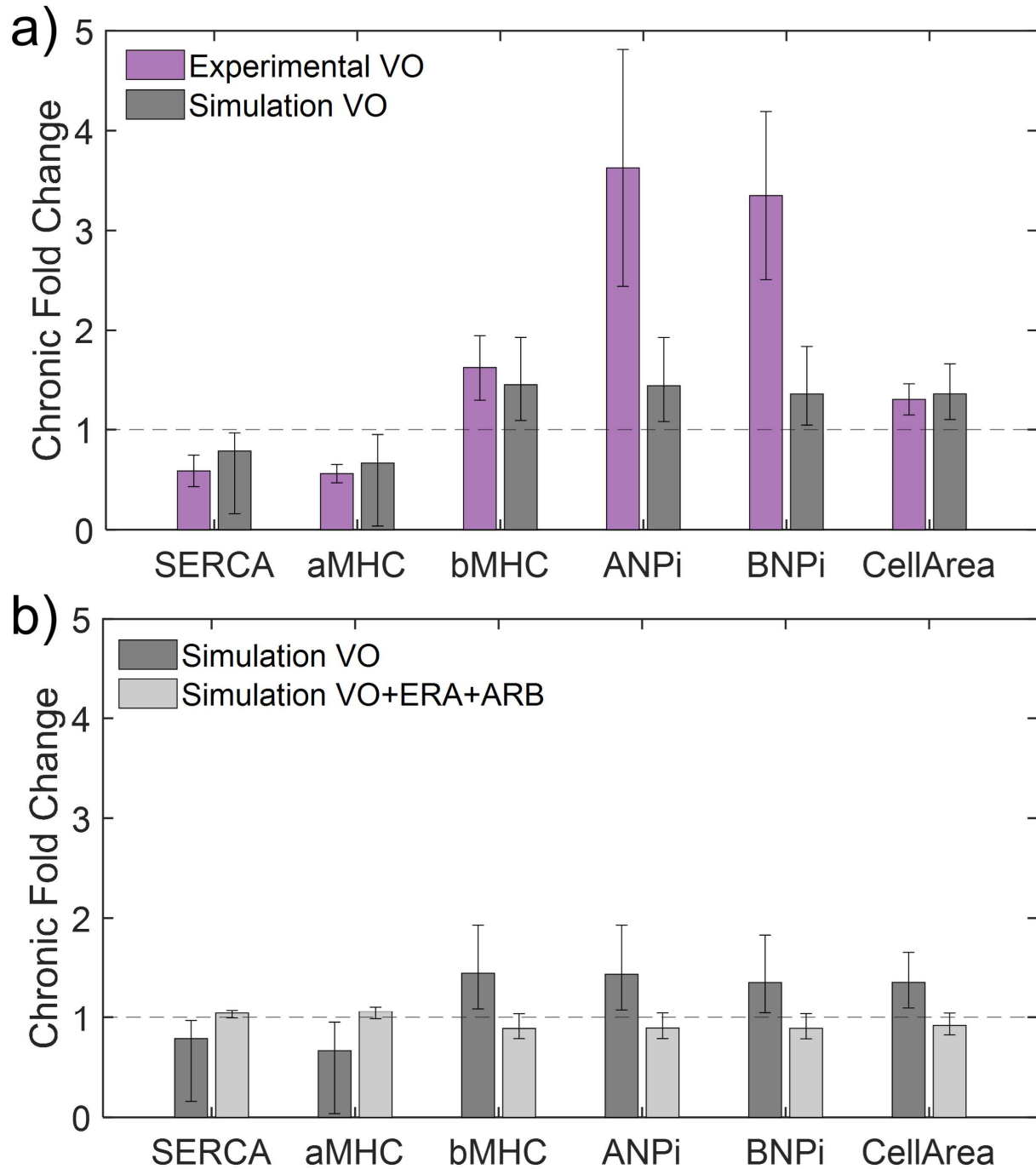
The model predictions of myocyte protein synthesis also quantitatively agree with the

magnitude of measured fold changes in SERCA, aMHC, and bMHC abundance in

cardiac tissue, but underestimate the magnitude of observed changed in ANP and BNP

485   (Fig 6a). Notably, our model reproduces the reported dephosphorylation of FAK and

486   decrease in Integrin activity during chronic volume overload (Supplementary figure

487   S1.9) [15–17]. This finding was independent of the choice of strain-to-myoStrain

488   mapping function. Rather, because integrins and FAK are directly downstream of

489   myoStrain in the network model, this result was a direct consequence of the data-driven

490   prediction that tissue-scale strain falls below its baseline in most cases of experimental

491   volume overload (Fig 5).

492
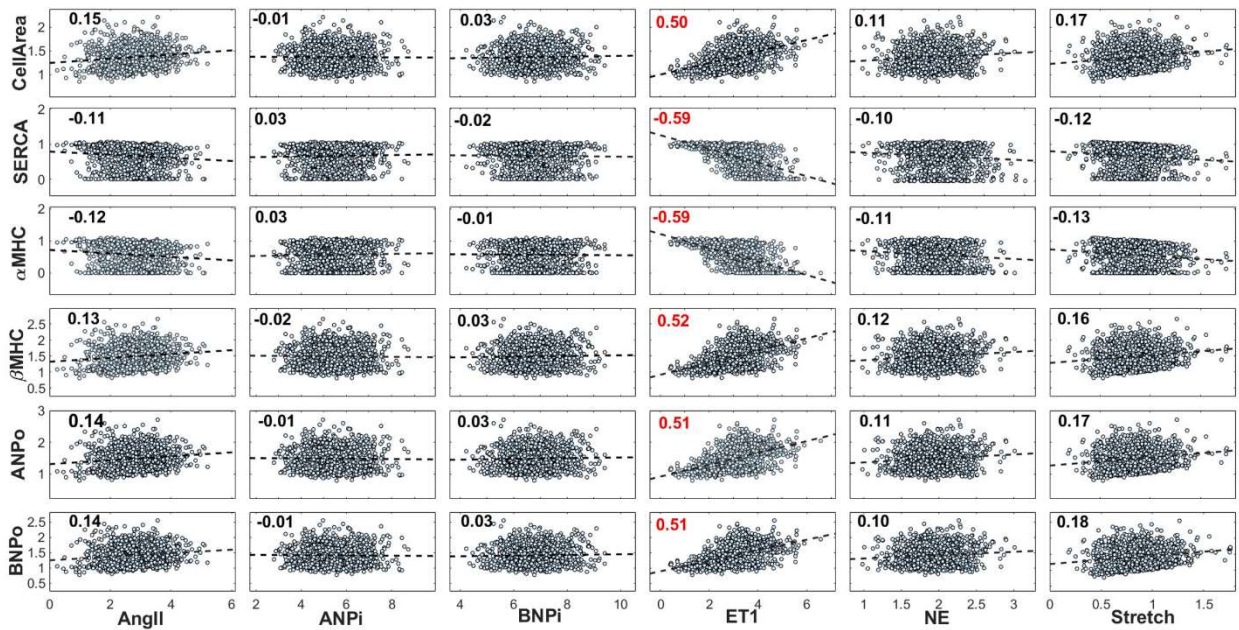
Fig 5. Diagram of cardiomyocyte signaling network model. The color-code indicates the logarithm of the fold change in activity of each node in chronic stages of VO respect to baseline, red means protein activity/abundance is above baseline and blue indicates protein activity/abundance falls below baseline.

Fig 6. Activity of network output nodes as representation of cardiomyocyte function. a) Validation of calibrated model predictions of network output nodes representing protein abundance of SERCA (Zheng et al. 2009) [17], aMHC, bMHC (Freire et al. 2007, Lachance et al. 2014) [49,50], ANP (Fareh et al. 1996) [51], BNP (Zheng et al. 2009, Fareh et al. 1996) and growth Cell Area (Urabe et al. 1992) [17,51,52]. The model (gray bars) shows good agreement with the trends observed from in vivo experiments in dogs and rats (purple bars). b) Effect of ERA+ARB treatment in the context of VO. The model predicts the combination of endothelin receptor antagonists (ERA) and angiotensin receptor blockers (ARB) has the potential to revert cardiac hypertrophy and inactivate the fetal gene program (light gray bars).

508 Next, we simulated published studies of chronic infusion of individual hormones that

509 play a role in volume-overload-induced growth. Sustaining elevated NE circulating

510 concentration 15.4 ± 1.9 fold times above normal levels for one month ($t/\tau = 0.7$)

511 produced a simulated growth of $26 \pm 9\%$, which is reasonably close to the reported

512 $20 \pm 5\%$ by King et al. [38]. Sustaining a circulating NE concentration 7.4 ± 0.9 fold

513 times above normal levels for 3 months ($t/\tau = 2.0.$) produced a simulated growth of

514 $33 \pm 17\%$, which was larger than the reported increase in LV mass of $15 \pm 6\%$ (Fig 7a).

515 It is important to highlight that these two studies evaluated both different concentrations

516 of NE and different time periods of infusion.

517
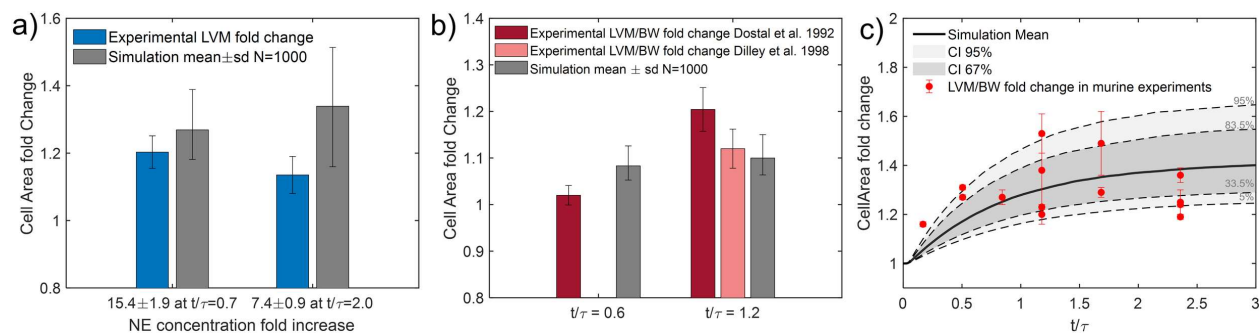
Fig 7. Validation of model predictions on the effect of growth factor infusions against
experimental data. a) Prediction of growth (gray bars) by infusion of NE against experiments in
dogs by King et al. (1987) (left blue bar) [38], and Laks et al (1973) (right blue bar) [37]. b)
Prediction of growth (gray bars) by ANGII infusion against experimental data by Dostal et al.
(1992) (dark red bars) and Dilley et al. (1998) (light red bars) [35,36]. c) Time-varying probability
distribution of growth by infusion of isoproterenol against experimental data in mice (red
markers), as compiled by Estrada et al. (2020) [40].

526 When we reproduced the ANGII infusion experiments by Dilley et al. and Griffin et al. by

527 imposing a fold-change increase in ANGII of 3.5 ± 0.3, the predicted cardiomyocyte

528 growth of $11 \pm 4\%$ agreed well with reported ventricular mass growth in both

529 experiments (Fig 7b). Simulating a saturating dose of ISO infusion in mice also

530   produced a cardiac growth curve that matched published data well, when the

531   characteristic growth time was scaled using the mice-to-dog heart rate ratio (Fig 7c).

532   3.6.   <u>Screening of pharmacological alternatives for treatment of VO</u>.

533   To explore possible therapeutic alternatives for the treatment of mitral regurgitation, we

534   simulated the effect of several interventions related to circulating hormones elevated

535   during VO. We simulated the effects of endothelin receptor blockers (ERA), angiotensin

536   receptor blockers (ARB), and β-blockers, administered throughout the course of VO

537   independently and in paired combinations. The largest mean effect of a single drug was

538   produced by ERA, which reduced CellArea growth from $35 \pm 24\%$ to only $6.5 \pm 11\%$, an

539   effect that is supported by empirical evidence (Fig 8a). In rat VO experiments, ERA

540   significantly reduced the LVM/BW ratio and reduced ventricular remodeling with respect

541   to controls [41–44,53]. By contrast, our model predicted that total blockade of the AT1

542   receptor would result in a $-10 \pm 40\%$ reduction in CellArea growth relative to untreated

543   controls, an effect that should be statistically undetectable given the high variability (Fig

544   8b). This result also agreed with negative results by Perry et al. and Dell'Italia et al. in

545   dogs and by Zhang et al. in rats, who reported that neither ARB nor angiotensin

546   converting enzyme inhibitors (ACEi) improved left ventricular function or significantly

547   reduced hypertrophy in experimental MR in dogs [26,46,54]. In dogs, β-blockers do not

548   produce any effect on ventricular mass in the first month of VO ($t/\tau < 0.7$) [55], but

549   chronic use of this drug ($t/\tau > 2.7$) appears to exacerbate hypertrophy in dog and rat

550   models of VO [14,16]. In our model, β-blockers produced a negligible mean effect

551   across all stages of VO (Fig 8c).

552
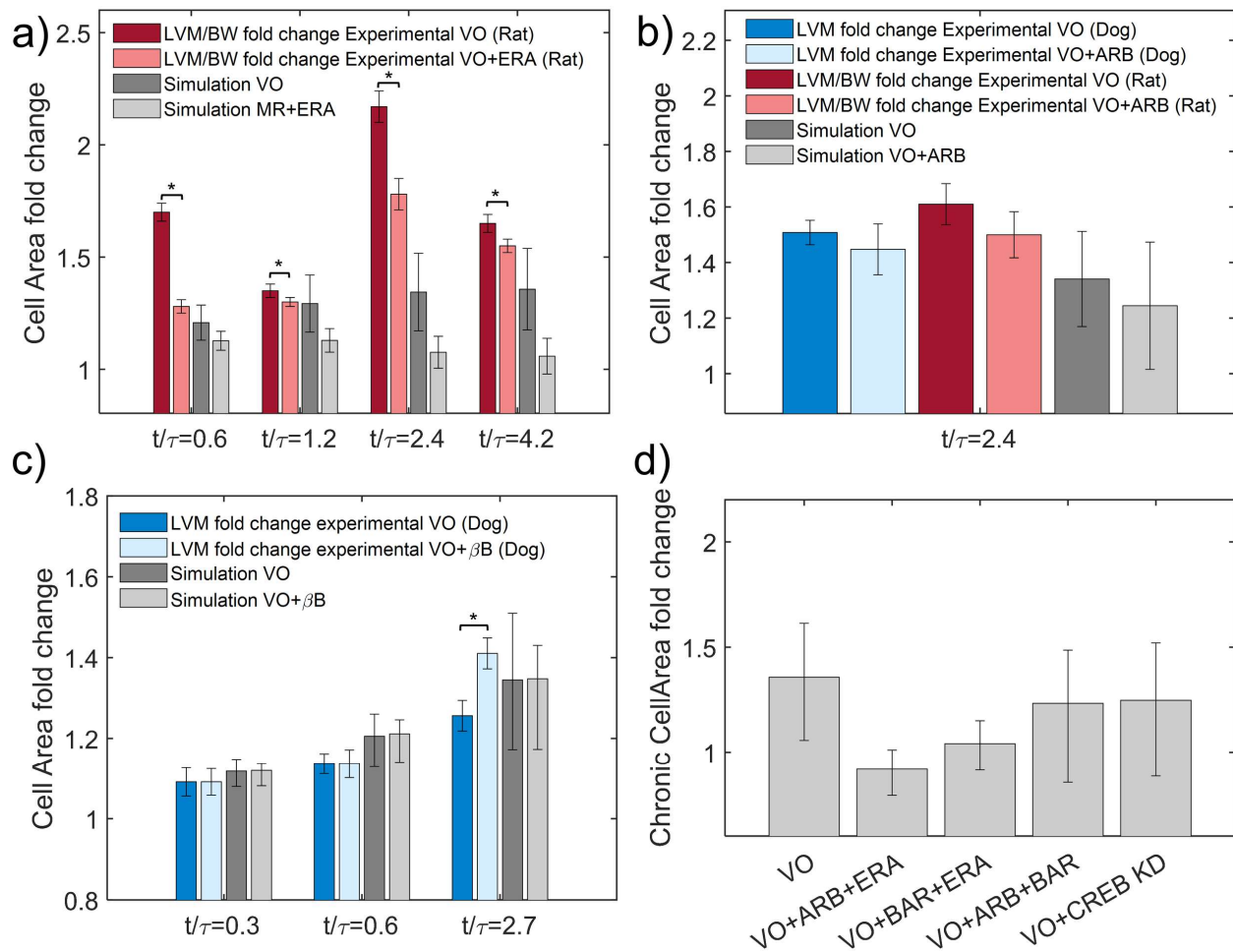
Fig 8. Model predictions on the effect of drug treatments in the context of VO. a) Predictions on the effect of endothelin receptor antagonist (ERA) on mass growth in VO (gray bars), and validation against experimental data on ERA treatment of VO in rats (red bars) by Francis et al. 2004 ($t/\tau = 0.6$), Murray et al. 2008 ($t/\tau = 1.2$), Lee et al. 2005 ($t/\tau = 2.4$), and Murray et al. 2009 ($t/\tau = 4.2$) [41–43,45]. b) Predictions on the effect of angiotensin II recepot blockers (ARB) on mass growth in VO (gray bars), and validation against experimental data on ARB treatment of VO in rats (red bars) by Zhang et al. 2010 [26,46], and in dogs (blue bars) by Perry et al. 2002 at $t/\tau = 2.4$. c) Predictions on the effect of β-blockers on mass growth in VO (gray bars), and validation against experimental data from dog models (blue bars) by Sabri et al. 2008 ($t/\tau \leq 0.6$) and Pat et al. 2008 ($t/\tau = 2.7$) [15,16]. d) Prediction on the effect of combined drug therapies and CREB knock down in chronic VO ($t/\tau = 3.0$) (light gray bars). ERA combinations, particularly ERA+ARB show largest potential to revert cardiac hypertrophy in VO. The * symbol indicates t-test statistical significance p<0.05.

When simulating pairwise combinations of these drugs, ERA plus ARB (ERA+ARB) produced the largest predicted effect on ventricular hypertrophy, returning CellArea to its original size and deactivating the fetal gene program (Fig 6b, 8d). In line with this

571 prediction, Leskinen et al. report the combination ERA+ARB blocked natriuretic peptide

572 synthesis by the cardiac tissue [56].

573 When we knocked down intermediate nodes individually in the context of simulated

574 volume overload. Only CREB knock-down produced a mean CellArea decrease larger

575 than 10%, with a total effect $-11 \pm 42\%$. However, the large variability suggests even

576 this effect would be undetectable in practice (Fig 8d). In the supplementary material

577 section S1.6. we compare how CREB knock-down performs against the blockade of

578 hormonal and mechanical stimuli, producing a similar mean effect on CellArea as ARB.

579 However, as CREB is located downstream the signaling reaction cascade, it has no

580 effects on intermediate signaling proteins (Supplementary figures S1.10, S1.12).

581 **4. Discussion**

582 This study used a Bayesian approach and well-established models of cardiac

583 hypertrophy to integrate a large body of experimental VO data in rats and dogs. The

584 resulting model can produce probabilistic predictions of cardiomyocyte hypertrophic

585 response to neurohormonal and mechanical stimulation, with an appropriate

586 propagation of experimental and model-induced uncertainty into the model's outputs.

587 The calibration against the activity of multiple signaling proteins in independent and

588 interconnected pathways enabled the adjustment of the relative influence of each

589 growth stimulus. The calibration was reasonably successful when tested against NE,

590 ISO, and ANGII infusions and the effect of various receptor blockers administered

591 during experimental VO.

592 The model identifies ET1 as one of the main drivers of hypertrophy in chronic stages of

593 VO. Consequently, the model predicts that the most effective strategies to block VO-

594 induced hypertrophy are combination therapies with multiple blockers including ERA,

595 especially with ARB, which mostly returns cardiomyocyte size to normal and deactivates

596 the fetal gene program.

597 The study of Leskinsen et al. 1997 and Fareh et al. 1996 on ERA+ARB effects on

598 neurohormonal profiling in VO in rats showed that the combined inhibition of both

599 receptors blocked the cardiac natriuretic peptide synthesis and reduced intracellular

600 Calcium concentration. The authors suggest that hormonal stimulation mostly regulates

601 cardiac secretion with myocyte stretch having marginal influence. The authors also

602 suggest that ET1 stimulation is more important in regulating the myocyte adaptative

603 response to VO than AngII [51,56]. Both observations confirm some of the most

604 prominent model predictions. Furthermore, according to several studies, ERA treatment

605 prevents cardiac growth and remodeling and cytokine expression in rat models of VO

606 [41–45]. Despite the apparent benefits of ERA in experimental VO and its proven

607 vasodilator effect, their clinical use has been limited by potentially severe side effects,

608 such as alterations of liver function, anemia, and edema. The most common clinical

609 application of ERA is to treat pulmonary artery hypertension, and recent efforts point to

610 the development of selective ERAs for treating persistent hypertension [57].

611 Our model suggests that the effect of NE as a growth factor is marginal in experimental

612 VO. The exaggerated NE concentration levels required by Laks et al. and King et al. to

613 produce LV mass increases below 20% support this notion [37,38]. In consequence, our

614 model predicts only negligible effects of β-blockade on cardiac hypertrophy at any stage

615 of VO. This prediction agrees well with observations in isolated cardiomyocytes, and

616 short-term experiments in vivo. However, chronic β-blockade during experimental VO

617 appears to exacerbate hypertrophy after several months in dogs [16,58,59]. We

618 hypothesize that this observation results from an indirect of β-blockade on hypertrophy

619 through modulating of LV contractility, an effect that is not included in the model

620 employed here. Evidence supporting that hypothesis includes the fact that β-blockade

621 partially restores FAK phosphorylation levels during experimental VO, indicating

622 increased activation of stretch-modulated hypertrophic pathways [14–16,60].

623 In clinical studies, β-blockers improves LV function, symptoms, and survival in patients

624 with chronic MR and heart failure (A. Ahmed & Dell'Italia, 2004; M. I. Ahmed et al.,

625 2012), but these benefits appear to be due to modulation of changes in signaling

626 pathways that occur with heart failure, effects not modeled in the present study.

627 One of the most interesting implications of our analysis is our prediction that in most

628 cases of VO, the combination of early overstretch and sustained neurohormonal

629 activation trigger sufficient hypertrophy to drive stretch below its baseline levels. This

630 prediction did not derive from the signaling network but rather from the Bayesian

631 approach to integrating published data on observed LV mass and volume increases

632 across a large number of experimental studies (Fig 2b,3c). This prediction may explain

633 the otherwise puzzling depression in the activity of key mechano-transduction proteins

634 in the context of volume overload. While FAK phosphorylation is elevated in pressure

635 overload and aortic valve regurgitation relative to baseline, FAK phosphorylation is

636 reduced in VO despite elevated LV volumes that are commonly assumed to indicate

637 elevated levels of myocyte stretch [15,16]. Interestingly, experiments on skeletal muscle

638 demonstrate that FAK dephosphorylation is a marker of mechanical unloading [61,62],

639 and the genetic restriction of FAK activity induces dilated thin-wall LV cardiomyopathy in

640   mice when challenged with pressure overload [63], evidence that stablishes an

641   interesting link between the dilated ventricle phenotype and mechano-transduction

642   depression. In previous work, we identified Ras as a relevant hub responsible for the

643   crosstalk of multiple pathways [20,29]. In the current work we found Ras was a critical

644   node integrating the competing effects of mechanical stretch and neurohormonal inputs

645   in VO. During early VO, elevated stretch and neurohormonal stimulation drove strong

646   activation of Ras, while in chronic VO reduced stretch was offset by continuing

647   neurohormonal stimulation, maintaining a low level of Ras activation (Fig 5,

648   Supplementary material 3).

649   **5. Limitations and future directions**

650   The ability to predict not only mean responses but also the uncertainty around those

651   predictions is a major advantage of Bayesian approaches. However, one important

652   limitation of the analysis presented here is that the range of uncertainty in our model

653   predictions is noticeably wider than the uncertainty in the experimental data used for

654   validation. Part of this predicted uncertainty is the inevitable consequence of integrating

655   disparate sources of data, which included the work of several research groups on

656   animals of different sizes and species and applying two different models of VO. Another

657   likely contributor is that we treated the levels of the various circulating hormones as

658   independent of each other; for example, some of our randomly selected parameter sets

659   will include extreme increases of AngII and low levels for the rest of the hormones.

660   However, in reality most reports suggest that the expression of these neurohormones is

661   correlated to the severity of cardiac insult, and therefore to each other. The current

662   model also lacks output-to-input feedback loops. For example, the strain-time curve is

663   imposed through random sampling, with no previous knowledge of the growth response,

664   and the CellArea likelihood is evaluated all available data on mass increases, not just

665   those occurring at a similar level of strain. Another limitation worth mentioning is that the

666   current model ignores the mechanical effects of neurohormonal alterations. Notably, the

667   drugs tested herein are known to have vasodilating effects, while AngII is a potent

668   vasoconstrictor, so changes in their concentrations modulate ventricular afterload. The

669   activity of adrenergic receptors modulates the muscular tone and contractile function of

670   the heart, thus potentially also modulating the mechanical strain. To address these

671   sources of variability, we can introduce additional experimental data and covariance

672   relations to the likelihood evaluation and incorporate this model of isolated

673   cardiomyocytes into a multiscale model of cardiovascular function. A multiscale model

674   could couple the amount of predicted cardiomyocyte growth to tissue and organ-scale

675   ventricular models to update the estimations of myocardial strain and introduce

676   feedback loops between systemic hemodynamics, neurohormonal alterations, drug

677   effects, and heart loading. One of the advantages of the Bayesian inference approach is

678   that all these proposed model improvements and data additions can be built on top of

679   the present work to narrow the range of predicted uncertainty.

680   We assumed changes in neurohormonal circulating concentrations are proportionally

681   transduced into receptor activity; this assumes large receptor availability and non-

682   competitive binding, neglects changes in receptor abundance, and ignores possible

683   differences in hormonal concentrations between the bloodstream and the immediate

684   cellular environment. Hormone concentrations in myocardial tissue extractions can be

685   several orders of magnitude larger than circulating concentration. However, they

686 showed similar trends, suggesting that the circulating and local values are at least

687 correlated (Dell'Italia et al., 1995, 1997; Tallaj et al., 2003). Ultimately, calibrating the

688 model to widely accessible data such as serum concentrations improves its translational

689 value.

6. Conclusions

691 We present a comprehensive data analysis of experimental data of volume overload

692 using a cardiomyocyte signaling model within a Bayesian inference framework. The

693 calibrated model suggests that growth in experimental VO is mostly driven by the

694 neurohormonal response, with the myocardial tissue stretch being compensated in early

695 stages of VO. The model suggests that Endothelin1 receptor activity plays a central role

696 in driving hypertrophic responses and the activation of the fetal gene program. The

697 model predicts the combination of ERA and ARB as a potential therapeutic alternative

698 to dampen cardiomyocyte hypertrophy and dysfunction in VO. Our model provides a

699 plausible explanation for the depression of mechano-transduction signaling pathway in

700 experimental VO, despite the widespread conception of volume overload hypertrophy

701 as driven by myocyte overstretch.

7. Acknowledgements

8. References

706 [1]   Wu S, Chai A, Arimie S, Mehra A, Clavijo L, Matthews R V., et al. Incidence and treatment of
707   severe primary mitral regurgitation in contemporary clinical practice. Cardiovascular
708   Revascularization Medicine 2018;19:960–3. https://doi.org/10.1016/J.CARREV.2018.07.021.

[2]   Carabello BA. The Current Therapy for Mitral Regurgitation. J Am Coll Cardiol 2008;52:319–26. https://doi.org/10.1016/J.JACC.2008.02.084.

[3]   Lorell BH, Carabello BA. Left Ventricular Hypertrophy. Circulation 2000;102:470–9. https://doi.org/10.1161/01.CIR.102.4.470.

[4]   Oyama MA. Neurohormonal activation in canine degenerative mitral valve disease: implications on pathophysiology and treatment. Journal of Small Animal Practice 2009;50:3–11. https://doi.org/10.1111/J.1748-5827.2009.00801.X.

[5]   Komajda M, Pousset F, Isnard R, Lechat P. The role of the neurohormonal system in heart failure. Heart 1998;79:S17. https://doi.org/10.1136/HRT.79.2008.17S.

[6]   Le Tourneau T, De Groote P, Millaire A, Foucher C, Savoye C, Pigny P, et al. Effect of mitral valve surgery on exercise capacity, ventricular ejection fraction and neurohormonal activation in patients with severe mitral regurgitation. J Am Coll Cardiol 2000;36:2263–9. https://doi.org/10.1016/S0735-1097(00)01015-9.

[7]   Chen HH, Schrier RW. Pathophysiology of Volume Overload in Acute Heart Failure Syndromes. Am J Med 2006;119:S11–6. https://doi.org/10.1016/J.AMJMED.2006.09.012.

[8]   Wilson K, Lucchesi PA. Myofilament dysfunction as an emerging mechanism of volume overload heart failure. Pflugers Arch 2014;466:1065–77. https://doi.org/10.1007/s00424-014-1455-9.

[9]   El Sabbagh A, Reddy YNV, Nishimura RA. Mitral Valve Regurgitation in the Contemporary Era: Insights Into Diagnosis, Management, and Future Directions. JACC Cardiovasc Imaging 2018;11:628–43. https://doi.org/10.1016/J.JCMG.2018.01.009.

[10]   Zheng J, Li Y, Billor N, Ahmed MI, Fang Y-HD, Pat B, et al. Understanding post-surgical decline in left ventricular function in primary mitral regurgitation using regression and machine learning models. Front Cardiovasc Med 2023;10. https://doi.org/10.3389/fcvm.2023.1112797.

[11]   Otto CM, Nishimura RA, Bonow RO, Carabello BA, Erwin JP, Gentile F, et al. 2020 ACC/AHA Guideline for the Management of Patients With Valvular Heart Disease: A Report of the American College of Cardiology/American Heart Association Joint Committee on Clinical Practice Guidelines. Circulation 2021;143:E72–227. https://doi.org/10.1161/CIR.0000000000000923.

[12]   Kerckhoffs RCP, Omens JH, McCulloch AD. A single strain-based growth law predicts concentric and eccentric cardiac growth during pressure and volume overload. Mech Res Commun 2012;42:40–50. https://doi.org/10.1016/j.mechrescom.2011.11.004.

[13]   Witzenburg CM, Holmes JW. A Comparison of Phenomenologic Growth Laws for Myocardial Hypertrophy. J Elast 2017;129:257–81. https://doi.org/10.1007/s10659-017-9631-8.

[14]   Seqqat R, Guo X, Rafiq K, Kolpakov MA, Guo J, Koch WJ, et al. Beta1-adrenergic receptors promote focal adhesion signaling downregulation and myocyte apoptosis in acute volume overload. J Mol Cell Cardiol 2012;53:240–9. https://doi.org/10.1016/J.YJMCC.2012.05.004.

[15]   Sabri A, Rafiq K, Seqqat R, Kolpakov MA, Dillon R, Dell'italia LJ. Sympathetic activation causes focal adhesion signaling alteration in early compensated volume overload attributable to isolated

746   mitral regurgitation in the dog. Circ Res 2008;102:1127–36.
747   https://doi.org/10.1161/CIRCRESAHA.107.163642.

748 [16] Pat B, Killingsworth C, Denney T, Zheng J, Powell P, Tillson M, et al. Dissociation between
749   cardiomyocyte function and remodeling with β-adrenergic receptor blockade in isolated canine
750   mitral regurgitation. Am J Physiol Heart Circ Physiol 2008;295:2321–7.
751   https://doi.org/10.1152/AJPHEART.00746.2008/ASSET/IMAGES/LARGE/ZH40120886060005.JPE
752   G.

753 [17] Zheng J, Chen Y, Pat B, Dell'Italia DLA, Tillson M, Dillon AR, et al. Molecular cardiology microarray
754   identifies extensive downregulation of noncollagen extracellular matrix and profibrotic growth
755   factor genes in chronic isolated mitral regurgitation in the dog. Circulation 2009;119:2086–95.
756   https://doi.org/10.1161/CIRCULATIONAHA.108.826230.

757 [18] Mohamed BA, Schnelle M, Khadjeh S, Lbik D, Herwig M, Linke WA, et al. Molecular and structural
758   transition mechanisms in long-term volume overload. Eur J Heart Fail 2016;18:362–71.
759   https://doi.org/10.1002/EJHF.465.

760 [19] Zeigler AC, Chandrabhatla AS, Christiansen SL, Nelson AR, Holmes JW, Saucerman JJ. Network
761   model-based screen for FDA-approved drugs affecting cardiac fibrosis. CPT Pharmacometrics Syst
762   Pharmacol 2021;10:377–88. https://doi.org/10.1002/PSP4.12599.

763 [20] Frank DU, Sutcliffe MD, Saucerman JJ. Network-based predictions of in vivo cardiac hypertrophy.
764   J Mol Cell Cardiol 2018;121:180–9. https://doi.org/10.1016/j.yjmcc.2018.07.243.

765 [21] Ross J, Sonnenblick EH, Taylor RR, Spotnitz HM, Covell JW. Diastolic Geometry and Sarcomere
766   Lengths in the Chronically Dilated Canine Left Ventricle. Circ Res 1971;28:49–61.
767   https://doi.org/10.1161/01.RES.28.1.49.

768 [22] Santamore WP, Burkhoff D. Hemodynamic consequences of ventricular interaction as assessed
769   by model analysis. American Journal of Physiology-Heart and Circulatory Physiology
770   1991;260:H146–57. https://doi.org/10.1152/ajpheart.1991.260.1.H146.

771 [23] Witzenburg CM, Holmes JW. Predicting the Time Course of Ventricular Dilation and Thickening
772   Using a Rapid Compartmental Model. J Cardiovasc Transl Res 2018;11:109–22.
773   https://doi.org/10.1007/S12265-018-9793-1.

774 [24] Dillon AR, Dell'Italia LJ, Tillson M, Killingsworth C, Denney T, Hathcock J, et al. Left ventricular
775   remodeling in preclinical experimental mitral regurgitation of dogs. Journal of Veterinary
776   Cardiology 2012;14:73–92. https://doi.org/10.1016/j.jvc.2012.01.012.

777 [25] Trappanese DM, Liu Y, McCormick RC, Cannavo A, Nanayakkara G, Baskharoun MM, et al.
778   Chronic β1-adrenergic blockade enhances myocardial β3-adrenergic coupling with nitric oxide-
779   cGMP signaling in a canine model of chronic volume overload: new insight into mechanisms of
780   cardiac benefit with selective β1-blocker therapy. Basic Res Cardiol 2015;110:456.
781   https://doi.org/10.1007/s00395-014-0456-3.

782 [26] Perry GJ, Wei CC, Hankes GH, Dillon SR, Rynders P, Mukherjee R, et al. Angiotensin II receptor
783   blockade does not improve left ventricular function andremodeling in subacute mitral

784   regurgitation in the dog. J Am Coll Cardiol 2002;39:1374–9. https://doi.org/10.1016/S0735-
785   1097(02)01763-1.

786 [27] Fomovsky GM, Clark SA, Parker KM, Ailawadi G, Holmes JW. Anisotropic reinforcement of acute
787   anteroapical infarcts improves pump function. Circ Heart Fail 2012;5:515–22.
788   https://doi.org/10.1161/CIRCHEARTFAILURE.111.965731.

789 [28] Spotnitz HM, Sonnenblick EH, Spiro D. Relation of Ultrastructure to Function in the Intact Heart:
790   Sarcomere Structure Relative to Pressure Volume Curves of Intact Left Ventricles of Dog and Cat.
791   Circ Res 1966;18:49–66. https://doi.org/10.1161/01.RES.18.1.49.

792 [29] Ryall KA, Holland DO, Delaney KA, Kraeutler MJ, Parker AJ, Saucerman JJ. Network reconstruction
793   and systems analysis of cardiac myocyte hypertrophy signaling. Journal of Biological Chemistry
794   2012;287:42259–68. https://doi.org/10.1074/jbc.M112.382937.

795 [30] Khalilimeybodi A, Paap AM, Christiansen SLM, Saucerman JJ. Context-specific network modeling
796   identifies new crosstalk in β-adrenergic cardiac hypertrophy. PLoS Comput Biol
797   2020;16:e1008490. https://doi.org/10.1371/journal.pcbi.1008490.

798 [31] Clark AP, Chowkwale M, Paap A, Dang S, Saucerman JJ. Logic-based modeling of biological
799   networks with Netflux. BioRxiv 2024:2024.01.11.575227.
800   https://doi.org/10.1101/2024.01.11.575227.

801 [32] Efendiev Y, Hou T, Luo W. Preconditioning Markov Chain Monte Carlo Simulations Using Coarse-
802   Scale Models. Https://DoiOrg/101137/050628568 2006;28:776–803.
803   https://doi.org/10.1137/050628568.

804 [33] Dhamala J, Arevalo HJ, Sapp J, Horácek BM, Wu KC, Trayanova NA, et al. Quantifying the
805   uncertainty in model parameters using Gaussian process-based Markov chain Monte Carlo in
806   cardiac electrophysiology. Med Image Anal 2018;48:43–57.
807   https://doi.org/10.1016/J.MEDIA.2018.05.007.

808 [34] Matsuo T, Carabello BA, Nagatomo Y, Koide M, Hamawaki M, Zile MR, et al. Mechanisms of
809   cardiac hypertrophy in canine volume overload. Am J Physiol Heart Circ Physiol 1998;275.
810   https://doi.org/10.1152/AJPHEART.1998.275.1.H65/ASSET/IMAGES/LARGE/AHEA40711007X.JPE
811   G.

812 [35] Dostal DE, Baker KM. Angiotensin II Stimulation of Left Ventricular Hypertrophy in Adult Rat
813   HeartMediation by the AT1 Receptor. Am J Hypertens 1992;5:276–80.
814   https://doi.org/10.1093/AJH/5.5.276.

815 [36] Dilley RJ, Nataatmadja I M. Heparin inhibits mesenteric vascular hypertrophy in angiotensin II-
816   infusion hypertension in rats. Cardiovasc Res 1998;38:247–55. https://doi.org/10.1016/S0008-
817   6363(98)00004-2/2/38-1-247-FIG5.GIF.

818 [37] Laks MM, Morady F, Swan HJC. Myocardial Hypertrophy Produced by Chronic Infusion of
819   Subhypertensive Doses of Norepinephrine in the Dog. Chest 1973;64:75–8.
820   https://doi.org/10.1378/chest.64.1.75.

821   [38]   King BD, Sack D, Kichuk MR, Hintze TH. Absence of hypertension despite chronic marked
822   elevations in plasma norepinephrine in conscious dogs. Hypertension 1987;9:582–90.
823   https://doi.org/10.1161/01.HYP.9.6.582.

824   [39]   Stewart JM, Patel MB, Wang J, Ochoa M, Gewitz M, Loud A V., et al. Chronic elevation of
825   norepinephrine in conscious dogs produces hypertrophy with no loss of LV reserve.
826   Https://DoiOrg/101152/Ajpheart19922622H331 1992;262:331–9.
827   https://doi.org/10.1152/AJPHEART.1992.262.2.H331.

828   [40]   Estrada AC, Yoshida K, Saucerman JJ, Holmes JW. A multiscale model of cardiac concentric
829   hypertrophy incorporating both mechanical and hormonal drivers of growth. Biomech Model
830   Mechanobiol 2021;20:293–307. https://doi.org/10.1007/s10237-020-01385-6.

831   [41]   Murray DB, McMillan R, Brower GL, Janicki JS. ETA selective receptor antagonism prevents
832   ventricular remodeling in volume-overloaded rats. Am J Physiol Heart Circ Physiol 2009;297:109–
833   16.
834   https://doi.org/10.1152/AJPHEART.00968.2008/ASSET/IMAGES/LARGE/ZH40070989120006.JPE
835   G.

836   [42]   Francis B, Winaver J, Karram T, Hoffman A, Abassi Z. Renal and systemic effects of chronic
837   blockade of ETA or ET B in normal rats and animals with experimental heart failure. J Cardiovasc
838   Pharmacol 2004;44. https://doi.org/10.1097/01.FJC.0000166214.42791.F2.

839   [43]   Lee DS, Kim DK, Choi SM, Kim YK, Ko BH, Jung YW. Bosentan Attenuates Compensatory Left
840   Ventricular Hypertrophy Induced by Aortocaval Fistula in Rats. Korean Circ J 2005;35:665.
841   https://doi.org/10.4070/kcj.2005.35.9.665.

842   [44]   Lüscher TF, Enseleit F, Pacher R, Mitrovic V, Schulze MR, Willenbrock R, et al. Hemodynamic and
843   neurohumoral effects of selective endothelin A (ETA) receptor blockade in chronic heart failure:
844   The heart failure ETA receptor blockade trial (HEAT). Circulation 2002;106:2666–72.
845   https://doi.org/10.1161/01.CIR.0000038497.80095.E1/ASSET/D1290F76-5B32-4F11-A37D-
846   58DB5407C8B6/ASSETS/GRAPHIC/G12FF1.JPEG.

847   [45]   Murray DB, Gardner JD, Brower GL, Janicki JS. Effects of nonselective endothelin-1 receptor
848   antagonism on cardiac mast cell-mediated ventricular remodeling in rats. Am J Physiol Heart Circ
849   Physiol 2008;294:1251–7.
850   https://doi.org/10.1152/AJPHEART.00622.2007/ASSET/IMAGES/LARGE/ZH40030881090005.JPE
851   G.

852   [46]   Zhang W, Elimban V, Xu YJ, Zhang M, Nijjar MS, Dhalla NS. Alterations of Cardiac ERK1/2
853   Expression and Activity Due to Volume Overload Were Attenuated by the Blockade of RAS.
854   Https://DoiOrg/101177/1074248409356430 2010;15:84–92.
855   https://doi.org/10.1177/1074248409356430.

856   [47]   Yoshida K, Holmes JW. Computational models of cardiac hypertrophy. Prog Biophys Mol Biol
857   2021;159:75–85. https://doi.org/10.1016/J.PBIOMOLBIO.2020.07.001.

858 [48] Caggiano LR, Holmes JW, Witzenburg CM. Individual variability in animal-specific hemodynamic
859   compensation following myocardial infarction. J Mol Cell Cardiol 2022;163:156–66.
860   https://doi.org/10.1016/j.yjmcc.2021.10.008.

861 [49] Freire G, Ocampo C, Ilbawi N, Griffin AJ, Gupta M. Overt expression of AP-1 reduces alpha myosin
862   heavy chain expression and contributes to heart failure from chronic volume overload. J Mol Cell
863   Cardiol 2007;43:465–78. https://doi.org/10.1016/J.YJMCC.2007.07.046.

864 [50] Lachance D, Dhahri W, Drolet MC, Roussel É, Gascon S, Sarrhini O, et al. Endurance training or
865   beta-blockade can partially block the energy metabolism remodeling taking place in experimental
866   chronic left ventricle volume overload. BMC Cardiovasc Disord 2014;14:1–11.
867   https://doi.org/10.1186/1471-2261-14-190/FIGURES/8.

868 [51] Fareh J, Touyz RM, Schiffrin EL, Thibault G. Endothelin-1 and Angiotensin II Receptors in Cells
869   From Rat Hypertrophied Heart. Circ Res 1996;78:302–11.
870   https://doi.org/10.1161/01.RES.78.2.302.

871 [52] Urabe Y, Mann DL, Kent RL, Nakano K, Tomanek RJ, Carabello BA, et al. Cellular and ventricular
872   contractile dysfunction in experimental canine mitral regurgitation. Circ Res 1992;70:131–47.
873   https://doi.org/10.1161/01.RES.70.1.131.

874 [53] Kala P, Gawrys O, Miklovič M, Vaňourková Z, Škaroupková P, Jíchová Š, et al. Endothelin type A
875   receptor blockade attenuates aorto-caval fistula-induced heart failure in rats with angiotensin II-
876   dependent hypertension. J Hypertens 2023;41:99–114.
877   https://doi.org/10.1097/HJH.0000000000003307.

878 [54] Dell'Italia LJ, Balcells E, Meng QC, Su X, Schultz D, Bishop SP, et al. Volume-overload cardiac
879   hypertrophy is unaffected by ACE inhibitor treatment in dogs.
880   Https://DoiOrg/101152/Ajpheart19972732H961 1997;273:961–70.
881   https://doi.org/10.1152/AJPHEART.1997.273.2.H961.

882 [55] Tallaj J, Wei C-C, Hankes GH, Holland M, Rynders P, Dillon AR, et al. β 1 -Adrenergic Receptor
883   Blockade Attenuates Angiotensin II–Mediated Catecholamine Release Into the Cardiac
884   Interstitium in Mitral Regurgitation. Circulation 2003;108:225–30.
885   https://doi.org/10.1161/01.CIR.0000079226.48637.5A.

886 [56] Leskinen H, Vuolteenaho O, Ruskoaho H. Combined Inhibition of Endothelin and Angiotensin II
887   Receptors Blocks Volume Load–Induced Cardiac Hormone Release. Circ Res 1997;80:114–23.
888   https://doi.org/10.1161/01.RES.80.1.114.

889 [57] Enevoldsen FC, Sahana J, Wehland M, Grimm D, Infanger M, Krüger M. Endothelin Receptor
890   Antagonists: Status Quo and Future Perspectives for Targeted Therapy. Journal of Clinical
891   Medicine 2020, Vol 9, Page 824 2020;9:824. https://doi.org/10.3390/JCM9030824.

892 [58] Nemoto S, Hamawaki M, De Freitas G, Carabello BA. differential effects of the angiotensin-
893   converting enzyme inhibitor lisinopril versus the beta-adrenergic receptor blocker atenolol on
894   hemodynamics and left ventricular contractile function in experimental mitral regurgitation. J Am
895   Coll Cardiol 2002;40:149–54. https://doi.org/10.1016/S0735-1097(02)01926-5.

896 [59] Tsutsui H, Spinale FG, Nagatsu M, Schmid PG, Ishihara K, DeFreyte G, et al. Effects of chronic
897   beta-adrenergic blockade on the left ventricular and cardiocyte abnormalities of chronic canine
898   mitral regurgitation. Journal of Clinical Investigation 1994;93:2639–48.
899   https://doi.org/10.1172/JCI117277.

900 [60] Nagatsu M, Zile MR, Tsutsui H, Schmid PG, DeFreyte G, Cooper IV G, et al. Native beta-adrenergic
901   support for left ventricular dysfunction in experimental mitral regurgitation normalizes indexes of
902   pump and contractile function. Circulation 1994;89:818–26.
903   https://doi.org/10.1161/01.CIR.89.2.818.

904 [61] Gao Y, Arfat Y, Wang H, Goswami N. Muscle atrophy induced by mechanical unloading:
905   Mechanisms and potential countermeasures. Front Physiol 2018;9:324534.
906   https://doi.org/10.3389/FPHYS.2018.00235/BIBTEX.

907 [62] Wisdom KM, Delp SL, Kuhl E. Use it or lose it: multiscale skeletal muscle adaptation to mechanical
908   stimuli. Biomech Model Mechanobiol 2015;14:195–215. https://doi.org/10.1007/s10237-014-
909   0607-3.

910 [63] Peng X, Kraus MS, Wei H, Shen TL, Pariaut R, Alcaraz A, et al. Inactivation of focal adhesion kinase
911   in cardiomyocytes promotes eccentric cardiac hypertrophy and fibrosis in mice. J Clin Invest
912   2006;116:217–27. https://doi.org/10.1172/JCI24497.

913

914

a)

Legend:
- ◇ Systole Baseline
- ● Diastole Baseline
- ● Diastole Acute Dilation
- ▲ Diastole Chronic Dilation
  10% LV mass increase

Axes: Sarcomere stretch vs LV Volume [ml]

b)

Legend:
- ● Baseline
- ● Acute Dilation
- ▲ Chronic Dilation
  10% LV mass increase
- ■ Chronic Dilation
  35% LV mass increase

Axes: Sphere stretch vs LV Volume [ml]

a)

b)

c)

d) $R^2 = 0.61$
$PCC = -0.78$
$p < 0.001$

a)

b)

c)